Supplementary Note 1: Bandstructure of ReS_2

The bandstructure of monolayer ReS_2 calculated using PBE functional is shown in Supplementary Figure 1a. Supplementary Figure 1b illustrates the first Brillouin zone of the monolayer ReS_2 unit cell with space group $P\bar{1}$[2]. The calculated bandgap is around 1.43 eV, though local or semi-local DFT is known to underestimate the bandgap of a material. However, the calculated bandstructure and the bandgap value closely matches earlier reports[1,2].

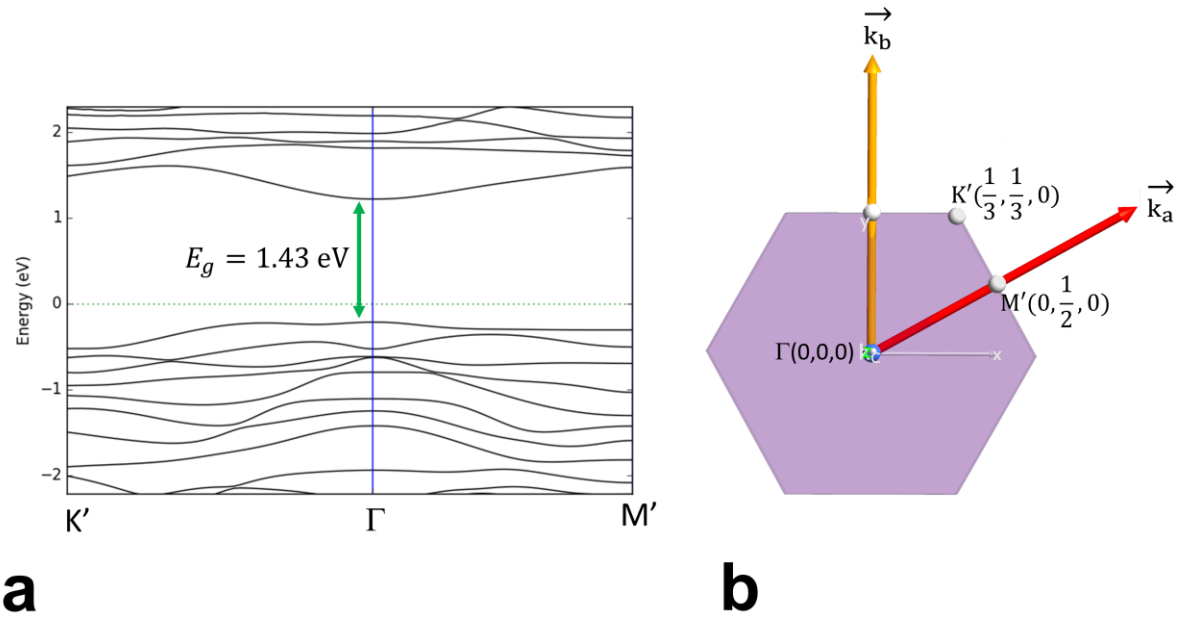

Supplementary Figure 1: Electronic structure of monolayer ReS_2. **a** Bandstructure and **b** the first Brillouin zone of monolayer ReS_2 unit cell.

Supplementary Note 2: Charge Difference Isosurface

Charge difference isosurface plots are a very useful tool in visualizing the transfer of charge over a 3D region. Supplementary Fig. 2 shows the top and side views of these plots for all 6 stable adsorption sites. The blue regions represent electron depletion and the green regions represent electron accumulation. It can be clearly seen that the Li gives away its charge to mostly 3 nearby S atoms, but in the case of α spots because of proximity to a metal atom a relatively low charge sharing between the Li and Re can be observed. Also, note from the

COHP analysis that α1 and α4 spots have equally less stiff Re atoms than α2 and α3 in the pristine material. This explains the relatively large amount of charge sharing between the Li and Re after lithiation at α1 and α4 and much less charge sharing at α2 and α3. Apparently, the less stiff Re atoms have been moved more by the lithiation process to form stronger bonds with the Li. The figure is illustrated on the next page.

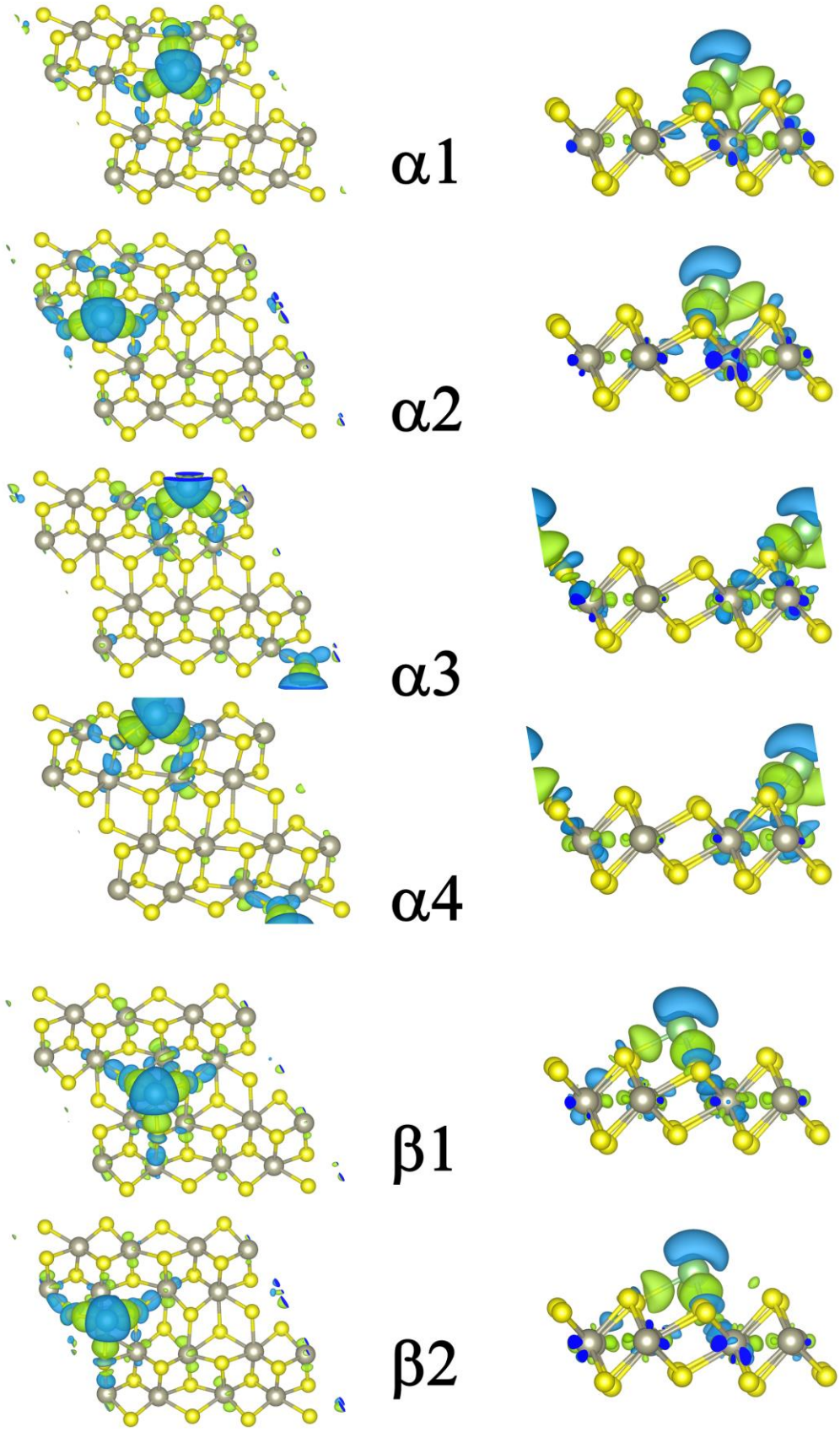

Supplementary Figure 2: Charge difference isosurface plots for all 6 stable binding sites. The charge difference isosurface is defined as $\Delta\rho = \rho_{ReS_2+Li} - \rho_{ReS_2} - \rho_{Li}$ where ρ_{ReS_2+Li}, ρ_{ReS_2} and ρ_{Li} are charge densities of ReS_2+Li system, ReS_2 substrate and Li adsorbate, respectively. Isosurface level is set at 0.002 eV/Å^3.

Supplementary Note 3: Detailed explanation of difference in binding energies of various sites

To explain the difference in binding energies of different adsorption sites we need to look closely at how Li binding in the material works. While being adsorbed, Li forms bonds with 3 neighboring chalcogen atoms and with a neighboring metal atom if one is available close-by. In order to tightly bind to the material, the Li tries move these atoms to modify the bond lengths which introduces distortion in the crystal. However, these chalcogen and metal atoms are tightly bound in the crystal by their neighboring atoms, which opposes this distortion. The more distortion the Li ion would be able to introduce in the substrate, the more negative the binding energy would be, i.e. the more tightly the Li will be able to bind to the material. If the chalcogen and the metal atoms, whom the Li ion is to form bonds with, are relatively tightly bound in the crystal, there will be less distortion induced by the lithiation process, which in turn will result in a weaker adsorption. We measure the amount of distortion induced by lithiation here as the sum of the displacement of all Re and S atoms. This is a relative quantity; the total atomic displacement in the substrate must be calculated as relative to another crystal structure with same lattice parameters and atomic configuration. Pristine ReS_2 structure seems like the best choice for this. However, the lithiation process changes the lattice parameters of the cell significantly which makes pristine ReS_2 an unsuitable choice for the reference. From our discussion above it follows that the binding site with least adsorption energy would make the least distorted structure which here would be the α4 site. We take this as the reference structure as the lattice parameters of all the lithiated cells with different binding sites are equal. As discussed in the main manuscript, we see that indeed the amount of stiffness in the possible binding sites affects binding energy adversely.

Supplementary Note 4: Non-unique MEPs between neighboring adsorption sites

Supplementary Figures 3-11 illustrate the possible non-unique minimum energy pathways between the neighboring binding sites. Note that by non-unique we mean that these MEPs go through another stable adsorption site as determined by our CINEB calculations. All possible unique MEPs between neighboring sites have been shown in Fig. 3 of the main manuscript.

The non-unique MEPs shown here are nothing but a combination of two unique MEPs. It should be noted that these non-unique MEPs are explored using a smaller number of images. By design, the climbing image in CINEB calculations converges to the highest energy saddle. Thus, in case of multiple-barrier MEPs, calculations can result in inaccurate barrier height for all barriers except the highest energy saddle. However, these calculations still confirm the presence of dual energy barriers in the MEPs and provide information on the intermediate stable adsorption sites they go through. As discussed in the main manuscript, because of periodic boundary condition there could be different MEPs between two adsorption sites, for diffusion to the left, right, upwards and downwards. For the convenience of visualization, Supplementary Fig. 3 shows a 2×2 ReS_2 unit cell with all possible adsorption sites and the related non-unique MEPs. Also, note that these non-unique paths between the neighboring sites are not exhaustive. We have not explored the MEPs which are obviously non-unique as all the unique paths have been explored in the main manuscript. For instance, the MEPs between the α sites through the inter-cluster region (white region in Supplementary Fig. 3) clearly would go through the nearest β sites and therefore have not been explored. The figures are shown from the next page.

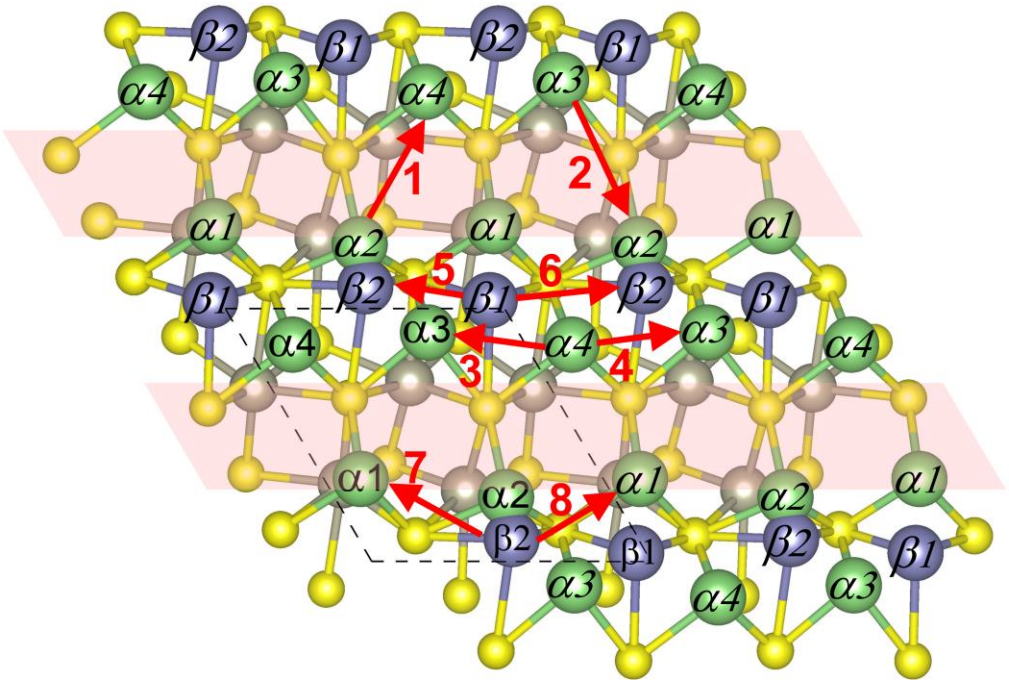

Supplementary Figure 3: A 2×2 ReS_2 unit cell with all adsorption sites and all of the following non-unique MEPs marked. Note that these non-unique MEPs always go through a different binding site other than the starting or destination site which would be too complex to capture in the figure. Thus, for illustration purpose the MEPs are represented with straight red arrows.

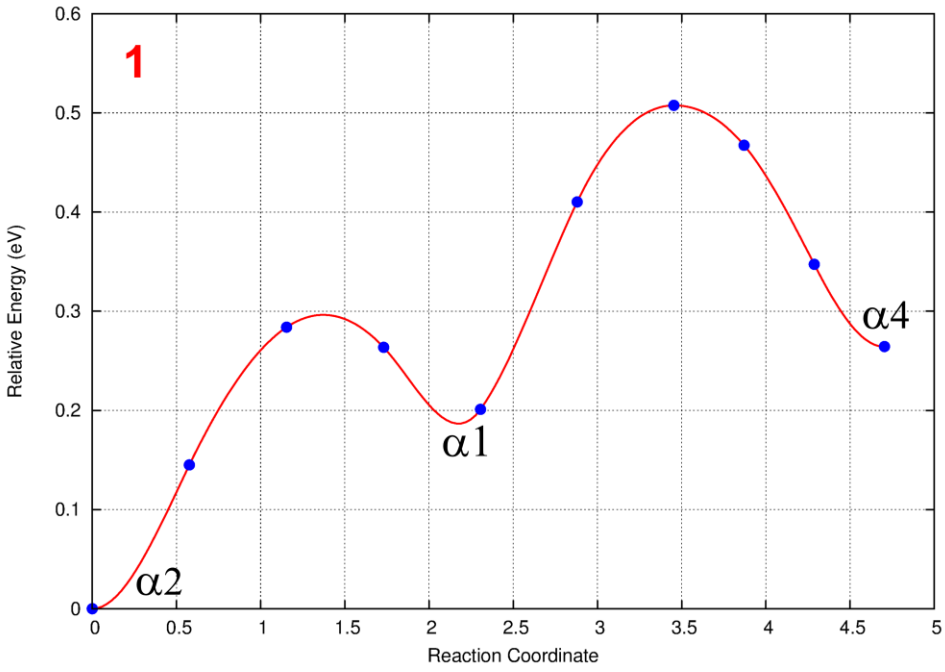

Supplementary Figure 4: Plot of the MEP between the binding sites α2 and α4 which goes through the site α1.

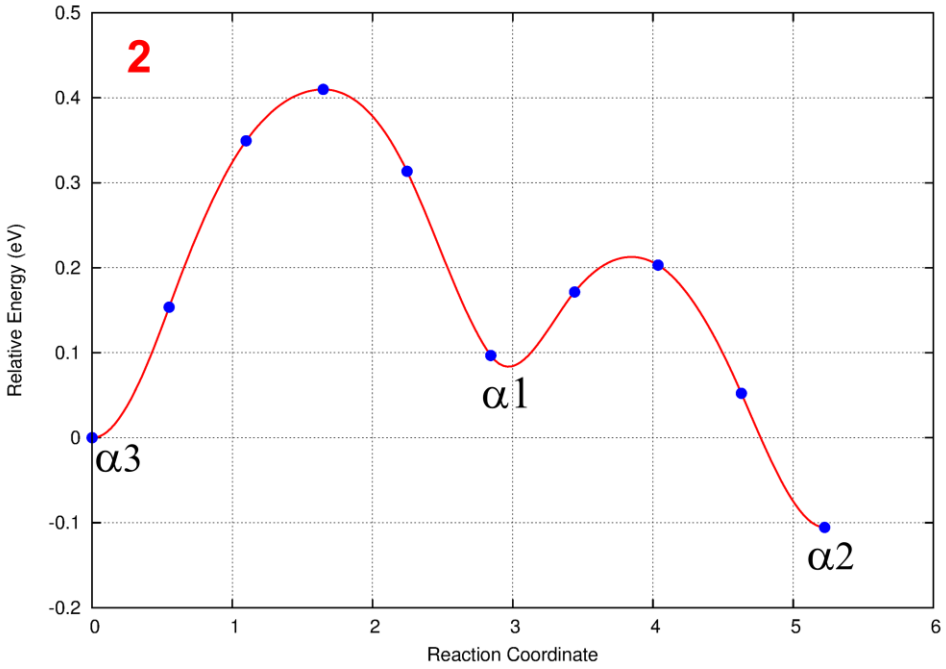

Supplementary Figure 5: Plot of the MEP between the binding sites α3 and α2 which goes through the site α1.

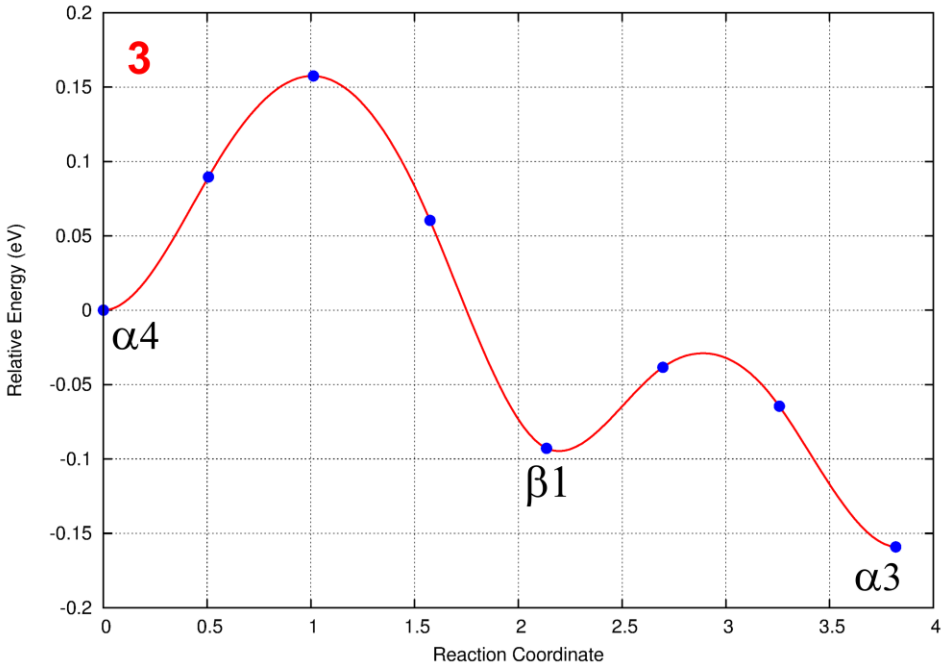

Supplementary Figure 6: Plot of the MEP to the left between the binding sites α4 and α3 which goes through the site β1.

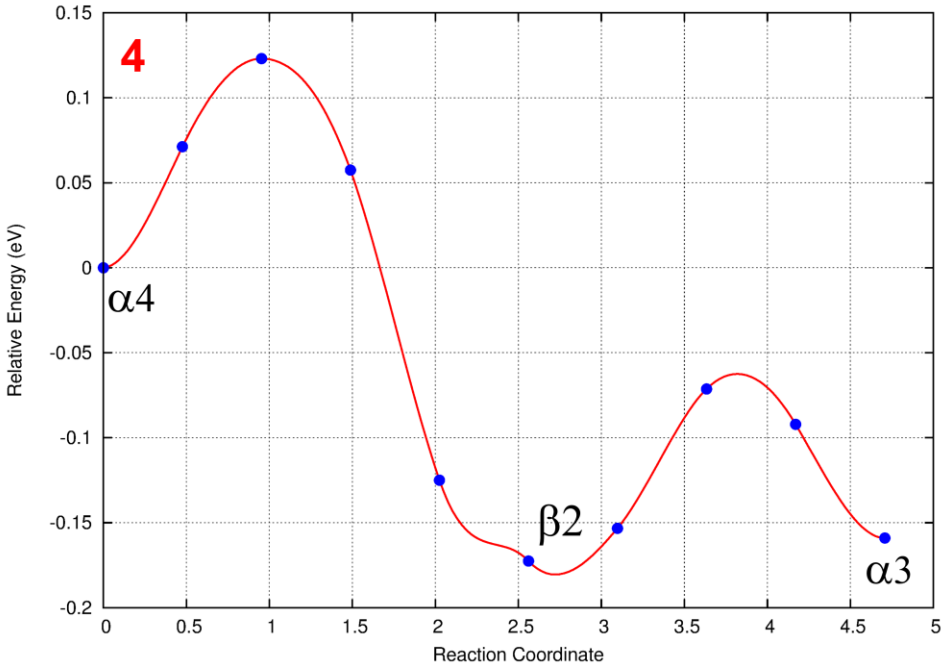

Supplementary Figure 7: Plot of the MEP to the right between the binding sites α4 and α3 which goes through the site β2.

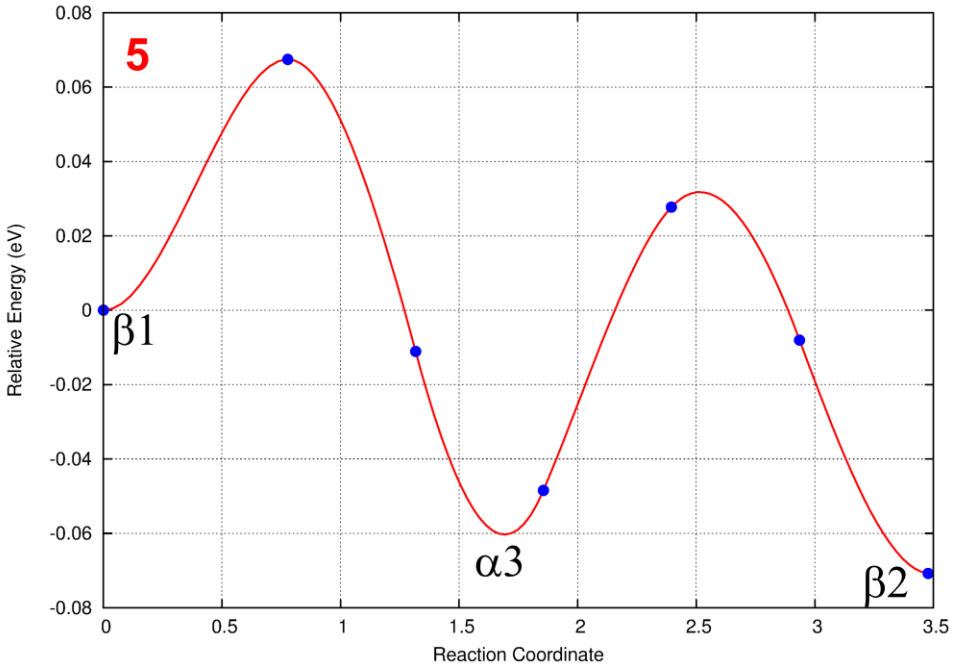

Supplementary Figure 8: Plot of the MEP to the left between the binding sites β1 and β2 which goes through the site α3.

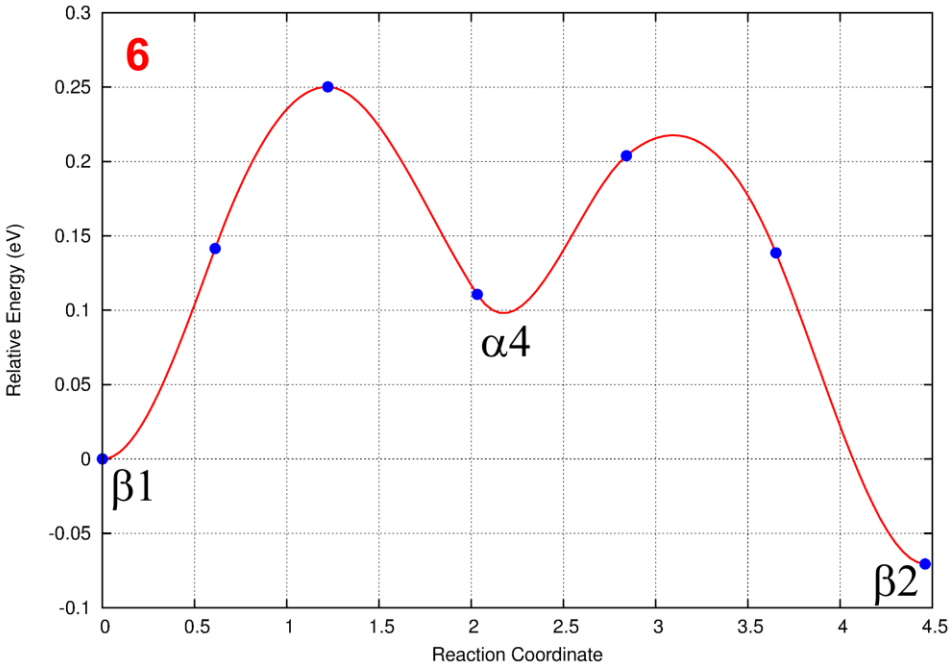

Supplementary Figure 9: Plot of the MEP to the right between the binding sites β1 and β2 which goes through the site α4.

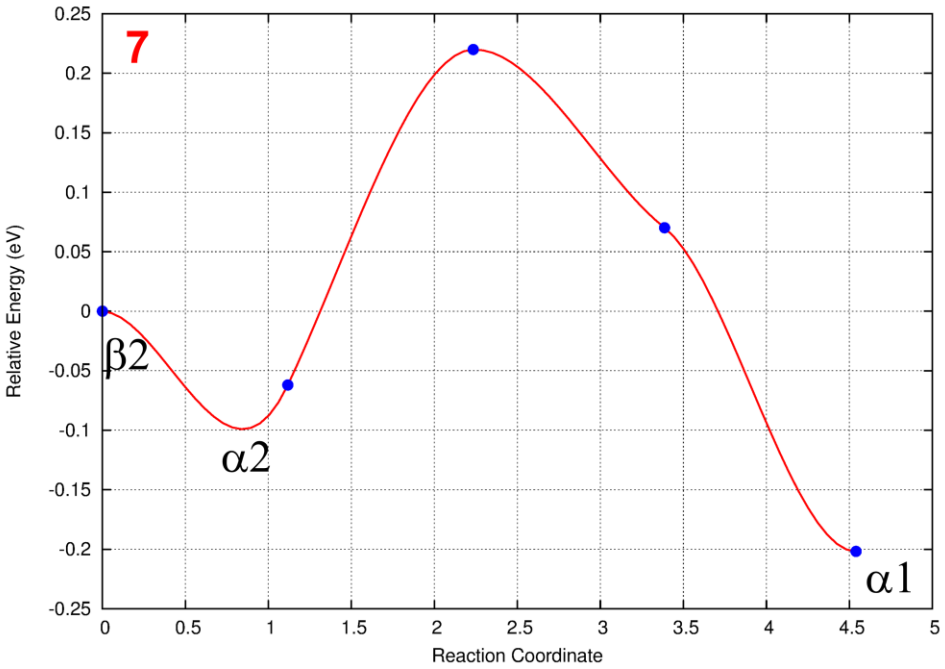

Supplementary Figure 10: Plot of the MEP to the left between the binding sites β2 and α1 which goes through the site α2.

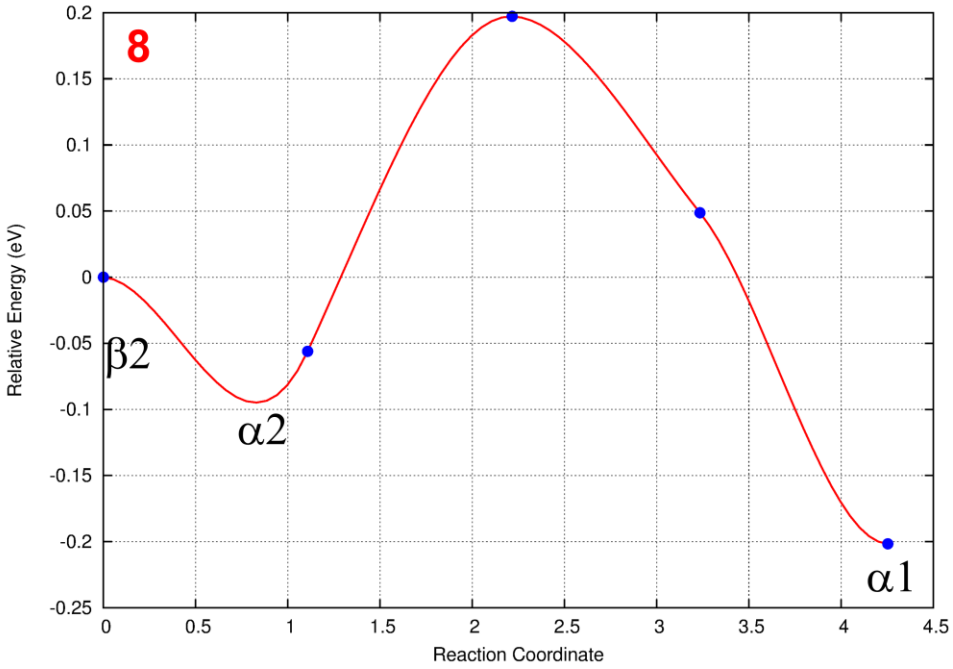

Supplementary Figure 11*:* Plot of the MEP to the right between the binding sites β2 and α1 which goes through the site α2.

Supplementary Note 5: Lithiated structures found by AIRSS

Supplementary Fig. 12 illustrates the lowest-energy phases for $Li_{0.125}ReS_2$, $Li_{0.250}ReS_2$ and $Li_{3.125}ReS_2$. Very low Li concentration (x = 0.125 and 0.25) do not seem to introduce significant amount of visible distortion into the crystal structure of ReS_2 while the $Li_{3.125}ReS_2$ phase seems completely amorphous with lots of broken Re-S bonds. Note that in $Li_{0.125}ReS_2$ and $Li_{0.250}ReS_2$ phases the adsorbed Li ions are so far apart that the coulombic repulsion between them is negligible. The figure is illustrated on the next page.

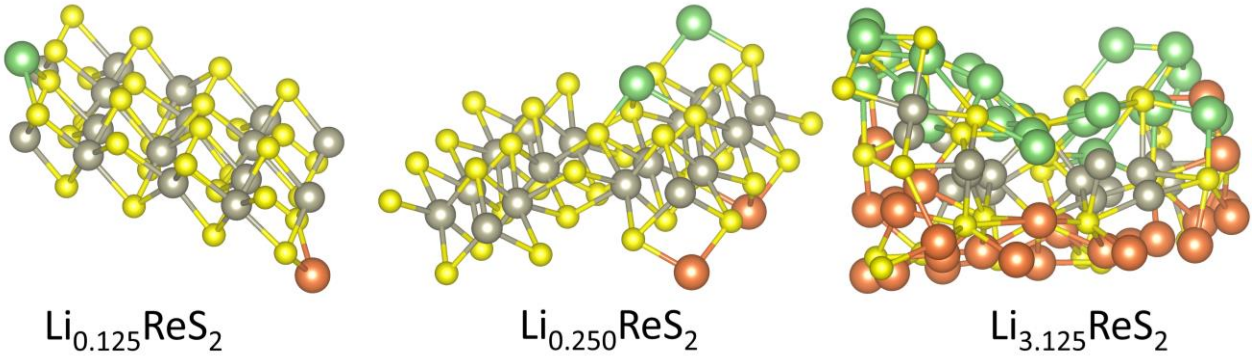

Supplementary Figure 12: AIRSS-found most stable phases of $Li_{0.125}ReS_2$, $Li_{0.250}ReS_2$ and $Li_{3.125}ReS_2$. Note that a tilted view of the first two structures are shown for clarity while in case of the third structure a pure side view is illustrated. The green balls represent Li ions on the top side of the substrate whereas the orange balls represent Li ions on the bottom.

Supplementary Note 6: COHP Plots

COHP plots of the pristine and all AIRSS-found lithiated phases can be found in Supplementary Fig. 13. Note that in the plots the COHP value is averaged over all the bonds in the phase. Therefore, the integration up to the fermi level of COHP values in these plots represents a measure of cohesive energy which can be seen declining with increasing Li content. Also, the band gap can be seen becoming almost zero at x = 1.0 indicating metallic conductivity. The figure is shown on the next page.

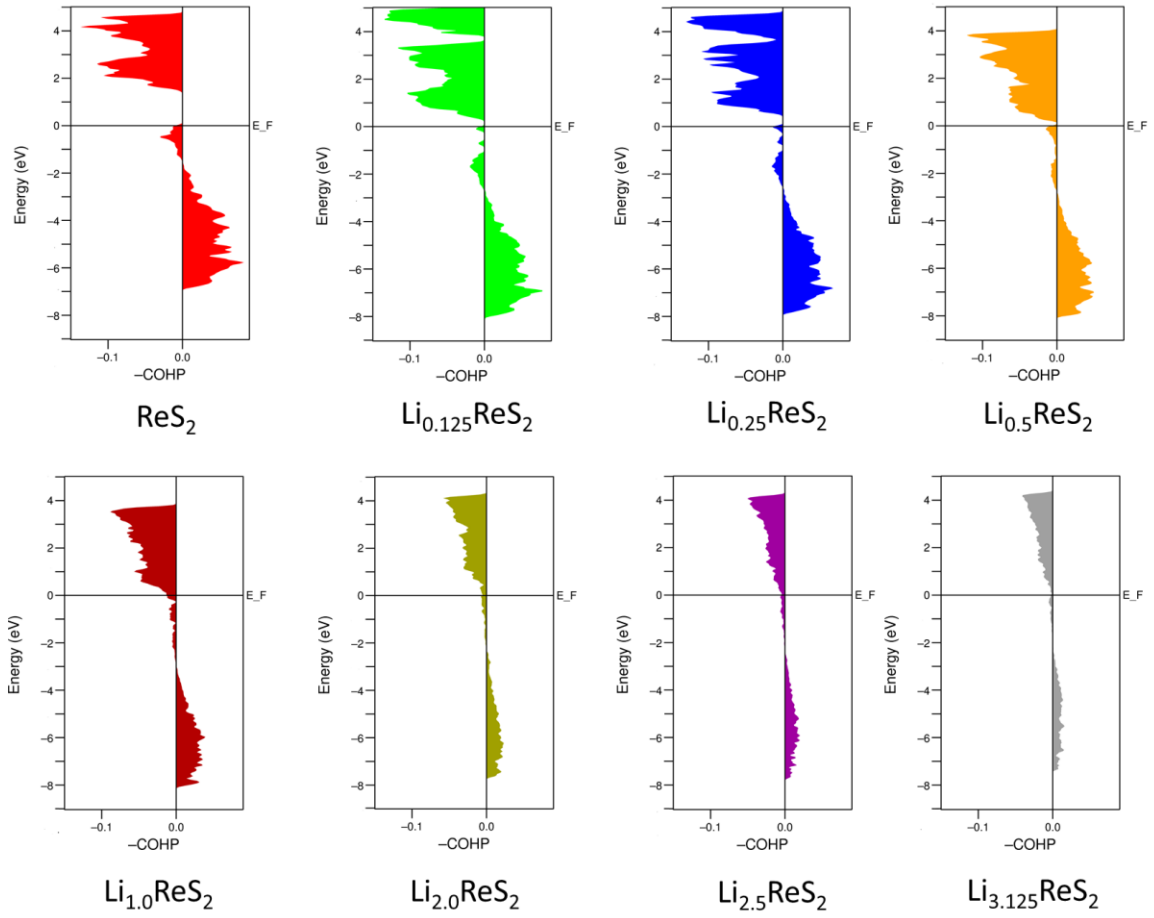

Supplementary Figure 13: COHP plots of the compound Li_xReS_2 where x = 0, 0.125, 0.25, 0.5, 1.0, 2.0, 2.5 and 3.125

Supplementary Note 7: Uniform adsorption

Supplementary Fig. 14 shows the uniformly Li adsorbed phase of Li_2ReS_2. In this phase E_{ads} = -0.64 eV and $E_{cohesive}$ = -4.06 eV whereas the AIRSS-found most stable Li_2ReS_2 phase has E_{ads} = -0.80 eV and $E_{cohesive}$ = -4.12 eV. Evidently, the AIRSS-found structure is more stable in terms of both adsorption and cohesive energy. However, the cohesive energy of the latter is only slightly lower and that could also be due to the fact that 3 'floating' Li ions have not been adsorbed in the substrate in the AIRSS-found phase.

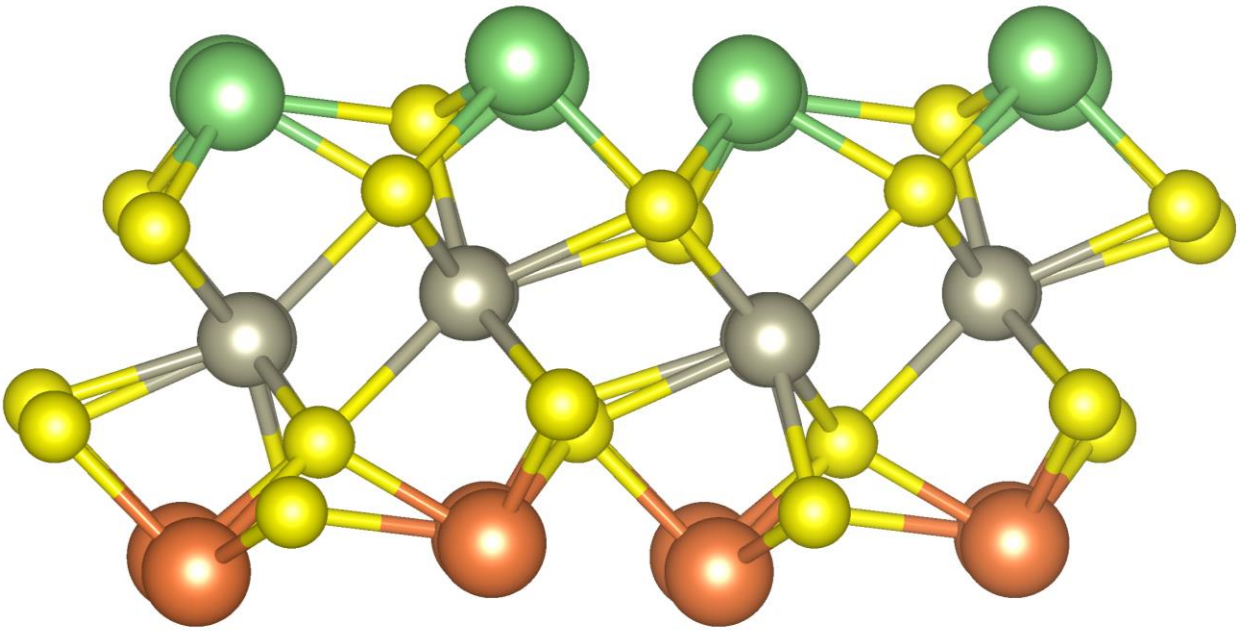

Supplementary Figure 14: Side view of uniformly Li adsorbed Li_2ReS_2 phase.

Supplementary Note 8: AIRSS Algorithm

The AIRSS algorithm we've used for lowest-energy lithiated structure finding is described on the next page. For n = 1, the algorithm remains same, only a single Li atom is placed over one surface instead of both sides. Supplementary Figures 15 and 16 illustrate the schematics of initial random structures generated by AIRSS with given constraints.

for n = 2, 4, 8, 16, 32, 40, 50

count = 0
while count <= 200

1. Generate a structure placing n/2 Li atoms on the one side of the material and n/2 Li atoms on the other side. x-y coordinates of the Li atoms are allowed to be completely random in the supercell while vertically the Li atoms are placed randomly in the range of 1.5-4.5 Å from the surface.
2. Keep track of the initial structure so that it's not generated again.
3. Send the structure to relax in the slave clusters with VASP.

if relaxation finishes successfully

1. Keep track of the total energy. Sort all structures by that.
2. count = count + 1
3. continue

else

continue

relax top few structures more rigorously.
analyze the top structure further.

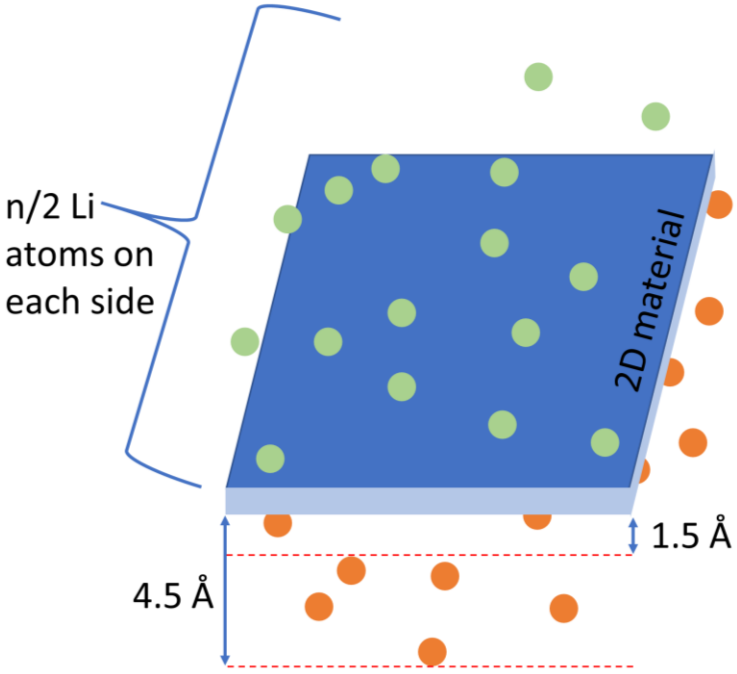

Supplementary Figure 15: Schematic representation of an initial configuration generated by AIRSS. The green balls represent Li ions on the top side of the substrate whereas the orange balls represent Li ions on the bottom.

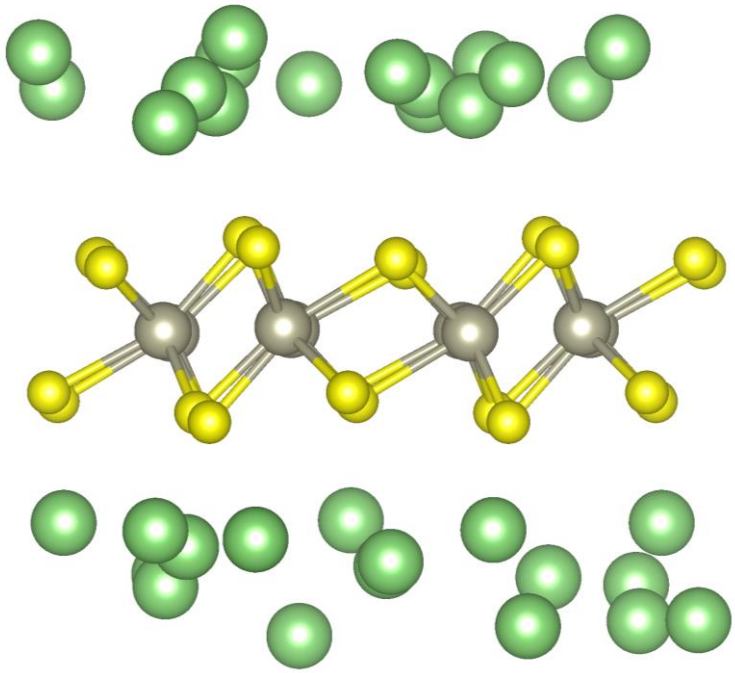

Supplementary Figure 16: A typical initial configuration generated by AIRSS for ReS_2 substrate. The green, gray and yellow balls represent the Li, Re and S atoms, respectively.

Supplementary Note 9: Computation time comparison between ReS_2 and MoS_2

Although ReS_2 unit cell is much larger than MoS2 unit cell[1,3], to make a fair assessment between their specific capacity, same supercell size is used for both. One of the salient features of our work is the use of heterogenous processor system to speed up the computation. To make an unbiased comparison between their computation time we conduct a separate study. We run AIRSS for Li_2MoS_2 and Li_2ReS_2 phases serially using 3 Xeon-Phi KNL (http://www.serc.iisc.in/facilities/cray-xc40-named-as-sahasrat/) nodes each. All other parameters, which can affect the calculation time such as k-points sampling, cutoff energy, smearing parameter, band parallelization etc. are kept same. Based on the initial 14 successfully relaxed structures for each, we find that Li_2MoS_2 structures have taken in average 1.61 hour to get relaxed, whereas it is more than double (3.40 hour) in case of Li_2ReS_2. As a result of including the same orbitals in the calculations as valence orbitals, our chosen Mo pseudopotential had 12 electrons, while Re pseudopotential had 13 electrons. However, the significant difference in average relaxation time probably is caused by the lack of symmetry in the ReS_2 structure. This timing comparison highlights the high computation budget required to work with ReS_2.

Supplementary Note 10: Delithiation

Since the delithiation algorithm described in the main manuscript is inherently random, there could be several delithiation paths depending on which Li ions are being removed in each step. In this section we will call this algorithm 'gradual delithiation'. In order to predict the reversibility of the lithiation-delithiation process, it must be confirmed that most of the random paths in the gradual delithiation algorithm would lead to similar results. Because of the high computational cost of this 'sequential' algorithm, we repeated the gradual delithiation process thrice while predicting the value of x_{max}. We found that indeed all the gradually delithiated structures are similar both visually and energetically. The other gradually delithiated structures are shown in Supplementary Fig. 17.

However, we have used another algorithm in this work to get a rapid estimate about which lithiated structures would return to the pristine phases. In this simple process, which we call 'quick delithiation', we remove all the Li atoms from the lithiated phase at once. Because this delithiation is too abrupt and the phase is very far away from its pristine form, we change the lattice parameters of the phase to that of its pristine substrate, i.e. the lattice parameters of the supercell before lithiation. The fractional co-ordinates of the atoms are kept fixed but the distances between them change according to the change in the lattice parameters. Then this structure is relaxed keeping the volume and shape of the cell fixed, i.e. only the atomic degrees of freedom are optimized. The results of this process are surprisingly similar to that of gradual delithiation albeit being computationally much lighter. All the quick delithiated structures are shown in Supplementary Fig. 18.

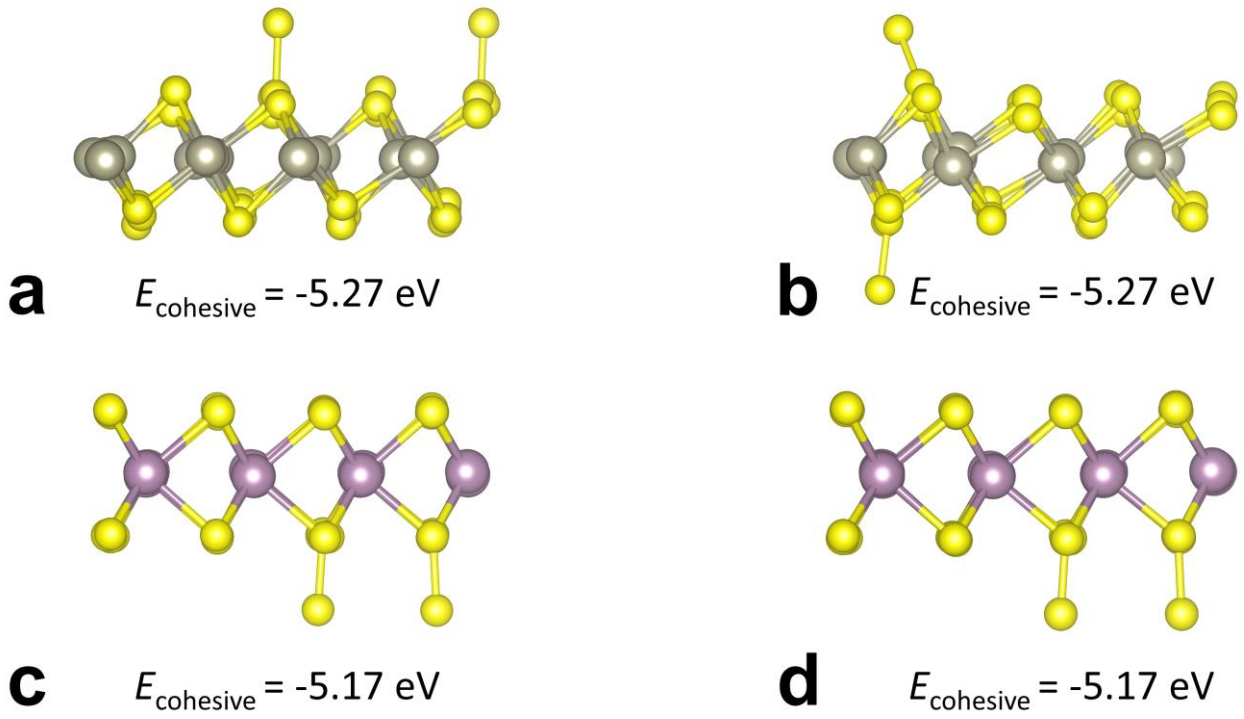

Supplementary Figure 17: Side view of gradually delithiated structures. **a**, **b** Li_2ReS_2 and **c**, **d** Li_2MoS_2 structures. The purple balls represent the Mo atoms.

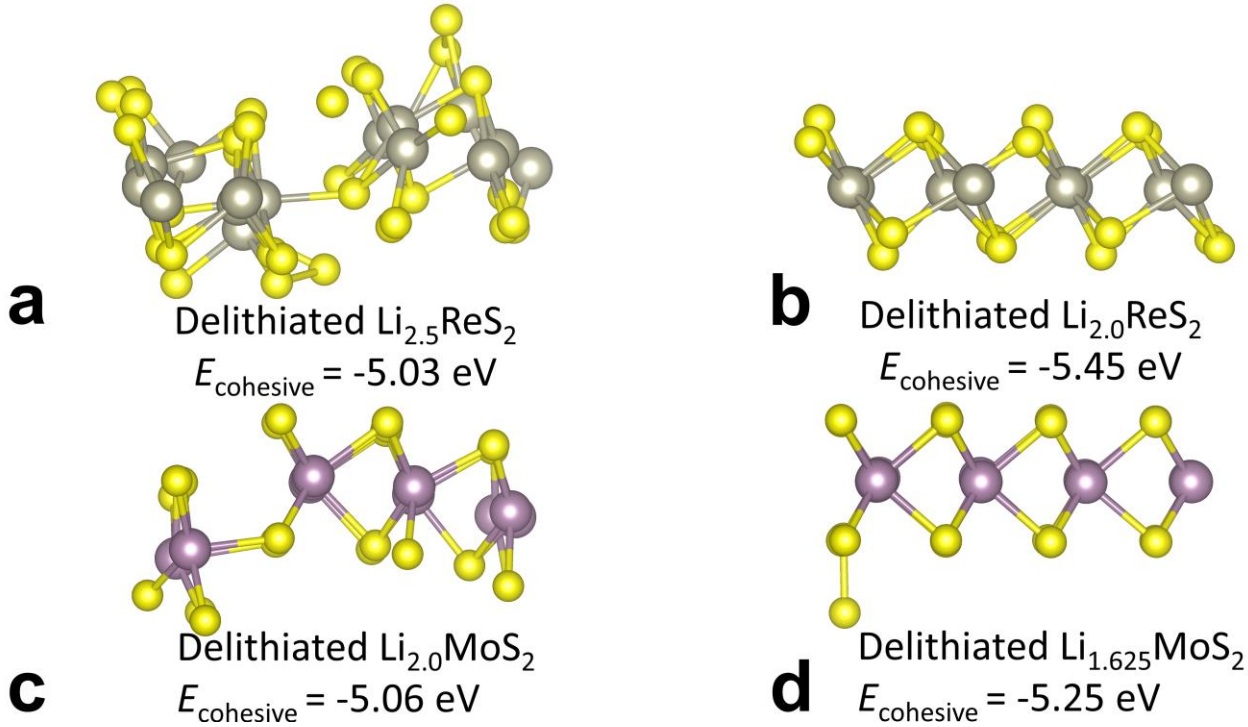

Supplementary Figure 18: Side view of quickly delithiated structures. **a** $Li_{2.5}ReS_2$, **b** Li_2ReS_2, **c** Li_2MoS_2 and **d** $Li_{1.625}MoS_2$ structures.

Supplementary References

1. Tongay, S. *et al.* Monolayer behaviour in bulk ReS_2 due to electronic and vibrational decoupling. *Nat. Commun.* **5,** 3252 (2014).
2. Yu, Z. G., Cai, Y. & Zhang, Y. W. Robust Direct Bandgap Characteristics of One-and Two-Dimensional ReS_2. *Sci. Rep.* **5,** 1–9 (2015).
3. Biswas, D. *et al.* Narrow-band anisotropic electronic structure of ReS2. *Phys. Rev. B* **96,** 085205 (2017).